

FORCE-GUIDED BRIDGE MATCHING FOR FULL-ATOM TIME-COARSENE DYNAMICS OF PEPTIDES

Ziyang Yu¹ Wenbing Huang^{3,4,*} Yang Liu^{1,2,*}

¹Department of Computer Science and Technology, Tsinghua University

²Institute for AI Industry Research (AIR), Tsinghua University

³Gaoling School of Artificial Intelligence, Renmin University of China

⁴Beijing Key Laboratory of Big Data Management and Analysis Methods, Beijing, China

yu-zy24@mails.tsinghua.edu.cn, hwenbing@126.com, liuyang2011@tsinghua.edu.cn

ABSTRACT

Molecular Dynamics (MD) simulations are irreplaceable and ubiquitous in fields of materials science, chemistry, pharmacology just to name a few. Conventional MD simulations are plagued by numerical stability as well as long equilibration time issues, which limits broader applications of MD simulations. Recently, a surge of deep learning approaches have been devised for time-coarsened dynamics, which learns the state transition mechanism over much larger time scales to overcome these limitations. However, only a few methods target the underlying Boltzmann distribution by resampling techniques, where proposals are rarely accepted as new states with low efficiency. In this work, we propose a force-guided bridge matching model, FBM, a novel framework that first incorporates physical priors into bridge matching for full-atom time-coarsened dynamics. With the guidance of our well-designed intermediate force field, FBM is feasible to target the Boltzmann-like distribution by direct inference without extra steps. Experiments on small peptides verify our superiority in terms of comprehensive metrics and demonstrate transferability to unseen peptide systems.

1 INTRODUCTION

Molecular Dynamics (MD) simulations are widely applied in the fields of materials science, physics, chemistry and pharmacology (Wolf et al., 2005; Durrant & McCammon, 2011; Salo-Ahen et al., 2020), which *in silico* models the dynamic mechanism of molecular systems at the atomic level. Accurate MD simulations enable the researcher to comprehend the equilibrium thermodynamics and kinetics of different molecular phases without the need for expensive wet-lab experiments, including protein folding (Lindorff-Larsen et al., 2011), deformation of nanocrystalline metals (Wolf et al., 2005), protein-ligand binding affinity (Wang et al., 2020) to name a few.

Conventional MD softwares, like AMBER (Pearlman et al., 1995) and CHARMM (Vanommeslaeghe et al., 2010), mostly pre-define an empirical force field of the molecular system and conduct simulations based on time integration of the Newtonian equation over time step Δt . For the stability of numerical integration, Δt should be dramatically small (typically 10^{-15} s), making it virtually impossible to capture vital

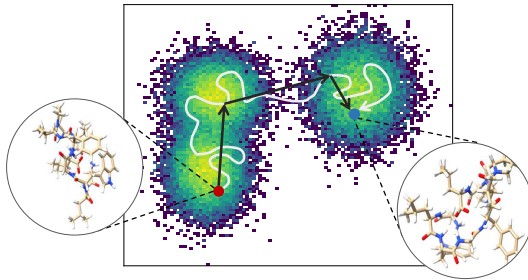


Figure 1: Illustration of how molecular conformations transfer from one state to another by MD (path in white) and time-coarsened dynamics (path in black).

*Corresponding authors: Wenbing Huang, Yang Liu.

phase transitions occurring on the microsecond scale (10^{-3} s) within a reasonable wall-clock time. Therefore, extending the temporal scale to unlock the potential of MD applications across various fields has become an urgent need.

A surge of approaches have been devised to tackle the temporal scale limitation. Some MD-like methods propose to modify the Potential Energy Surface (PES) or effective temperature for effective rare event sampling, such as temperature-accelerated dynamics (Voter et al., 2000), Gaussian accelerated MD (Pang et al., 2017), and metadynamics (Laio & Parrinello, 2002). Another class of methods take the advantage of Monte Carlo (MC) steps that enable quicker transition across free energy basins, including parallel Monte Carlo (Sadigh et al., 2012), replica-exchange MD (Sugita & Okamoto, 1999), and force bias Monte Carlo (Neyts & Bogaerts, 2014). However, all these methods share the same limitation: different molecular systems require different simulations to be performed. Intrinsically, many atomistic systems showcase related dynamic patterns since particles are all governed by the interatomic potential as well as the rules of physics.

Here we focus on Machine Learning (ML) methods that boost the MD simulation. In contrast to the time integration, the data-driven paradigm provides some more flexible ways to learn dynamics and transferability across different molecular systems. The time-coarsened dynamics as illustrated in Figure 1, one effective solution where the model is proposed to learn the conditional transition distribution over a much larger time step $\tau \gg \Delta t$, is widely adopted by Timewarp (Klein et al., 2024), ITO (Schreiner et al., 2024), and Score Dynamics (Hsu et al., 2024). However, none of these methods are designed to target the equilibrium distribution (*i.e.*, the Boltzmann distribution), and due to the biased data distribution, the configurations inferred directly from the model will also be biased, which is inconsistent with thermodynamic principles. Timewarp employs the Metropolis-Hastings algorithm (Metropolis et al., 1953) to resample from the equilibrium distribution, yet the unbearably low acceptance rate still hinders its applicability.

In this work, we propose Force-guided Bridge Matching (FBM), a novel ML-based approach that combines bridge matching and intermediate force field for full-atom time-coarsened dynamics to target the Boltzmann-like distribution. Our main contributions are:

1. To our best knowledge, we present the first full-atom, conditional generative model that directly samples from the Boltzmann-like distribution without resampling procedures.
2. We demonstrate that FBM exhibits transferability to unseen peptide systems.
3. We conduct fair comparisons of ML-based methods in a time-coarsened manner, where FBM consistently demonstrates state-of-the-art results across various test peptides.

2 RELATED WORK

Boltzmann Generator An important objective of MD research is to quickly sample from the Boltzmann distribution, thereby revealing the free energy landscape and distinctive phases of matter of molecular systems in thermodynamic equilibrium. *Boltzmann generators* (Noé et al., 2019; Köhler et al., 2021; 2023; Falkner et al., 2023; Klein et al., 2024; Klein & Noé, 2024) employ generative models to produce samples asymptotically from the Boltzmann distribution mainly by: (i) Apply reweighting techniques to i.i.d. generated samples. (ii) Inference in a Markov Chain Monte Carlo (MCMC) procedure. These approaches heavily rely on MC resampling techniques, which are the bottleneck of the sampling efficiency due to costly energy calculation and low acceptance rates. Most similarly to our work, Wang et al. (2024) propose ConfDiff that incorporate the energy and force guidance directly into score diffusion to target the Boltzmann-like distribution, yet it only works well on protein backbones and takes an unconditional way that fails to capture time dynamics. In contrast, FBM introduces the force guidance into the bridge matching framework, making it possible to sample straightforwardly from the Boltzmann-like distribution and learn how molecular systems evolve over time.

Time-Coarsened Dynamics To overcome the instability of numerical integration with longer time steps, many deep learning methods have adopted the idea of learning the conditional probability distribution over larger temporal scales to accelerate MD simulations, namely *time-coarsened dynamics*. Fu et al. (2023) proposes a multi-scale graph network to learn long time dynamics of polymers, which does not operate in the all atom system. ITO (Schreiner et al., 2024) is devised to learn the

transition probability over multiple time resolutions, yet its transferability across chemical space should be further explored. Recently, Timewarp (Klein et al., 2024) and TBG (Klein & Noé, 2024) utilize augmented normalizing flows and flow matching respectively for transferable time-coarsened dynamics of small peptides, while both need additional reweighting procedures to debias expected values from the Boltzmann distribution. Moreover, Score Dynamics (Hsu et al., 2024) applies the score diffusion mechanism to capture dynamics without targeting the Boltzmann distribution. On the contrary, FBM is designed to learn time-coarsened dynamics at the atomic level and target the Boltzmann-like distribution during the inference procedure, which shows transferability to unseen peptides as well.

3 PRELIMINARIES

Bridge Matching *Bridge matching* (Shi et al., 2024) is a generative framework that learns a mimicking diffusion process between two arbitrary distributions, allowing for more flexible choices of priors and sampling methods. Denote \mathbb{Q}_0 the prior distribution, \mathbb{Q}_1 the data distribution and $t \in [0, 1]$ the continuous diffusion time, then define the forward noising process:

$$d\mathbf{X}_t = f_t(\mathbf{X}_t)dt + \sigma_t d\mathbf{B}_t, \mathbf{X}_0 \sim \mathbb{Q}_0, \quad (1)$$

where \mathbf{X}_t and \mathbf{B}_t are the random variable and the Brownian motion of the process at time t , respectively. Given this process is pinned down at an initial and terminal point x_0, x_1 , the conditional distribution $\mathbb{Q}_{|0,1}(\cdot|x_0, x_1)$ will be represented as a *diffusion bridge* in the form of $d\mathbf{X}_t = \{f_t(\mathbf{X}_t) + \sigma_t^2 \nabla \log \mathbb{Q}_{|0,1}(x_1|\mathbf{X}_t)\}dt + \sigma_t d\mathbf{B}_t$ with $\mathbf{X}_0 = x_0$, where Doob h -transform theory (Rogers & Williams, 2000) guarantees $\mathbf{X}_1 = x_1$. For simplification, considering $f_t = 0$ and $\sigma_t = \sigma$, the process will degenerate to the *Brownian bridge* $d\mathbf{X}_t = \frac{x_1 - \mathbf{X}_t}{1-t}dt + \sigma d\mathbf{B}_t$.

4 METHOD

In this section, we will present the full operational workflow of our Force-guided Bridge Matching (FBM) for time-coarsened dynamics on peptides. In § 4.1 we will demonstrate the details of representing molecules (*i.e.*, peptides) as graph structures at the atomic level and provide the task formulation subsequently. In § 4.2, we first train a conditional generative framework based on bridge matching as the baseline model, which learns the time-coarsened dynamics from the biased distribution. We further propose a novel framework targeting the Boltzmann-like distribution by incorporating the intermediate force field into the baseline model in § 4.3. The architecture of neural networks employed in our model is further introduced in § C, and all proofs of propositions are provided in § B.

4.1 MOLECULAR REPRESENTATION

We represent each peptide as a graph $\mathcal{G} = (\mathcal{V}, \mathcal{E})$ consisting of the node set \mathcal{V} and the edge set \mathcal{E} . For a peptide with N atoms (including hydrogens), $\mathcal{V} = \{v_0, \dots, v_{N-1}\}$ where v_i ($0 \leq i < N$) represents the i -th atom of the molecule. Here, we emphasize that the graph remains isomorphic against the permutation of \mathcal{V} , thereby satisfying permutation invariance. Each node v_i is further attributed with Cartesian coordinates $\vec{x}_i \in \mathbb{R}^3$ from the structural information and node features $z_i \in \mathbb{R}^H$ from the embedding of atom types, where H represents the hidden dimension. Since most peptides (and proteins) are composed of 20 natural amino acids and exhibit similar and regular features in their molecular conformations, we construct the atom type vocabulary based on the atom nomenclature of Protein Data Bank (Berman et al., 2000) to obtain more refined atomic representations. Finally, features and Cartesian coordinates of all nodes are concatenated for the overall node representation:

$$\vec{\mathbf{X}} = [\vec{x}_0, \dots, \vec{x}_{N-1}]^\top \in \mathbb{R}^{N \times 3}, \mathbf{Z} = [z_0, \dots, z_{N-1}]^\top \in \mathbb{R}^{N \times H}. \quad (2)$$

Edges of the graph are constructed with the cutoff hyperparameter r_{cut} . For any node pair v_i, v_j ($0 \leq i < j < N$), the connection is established iff $\|\vec{x}_i - \vec{x}_j\| < r_{\text{cut}}$. We claim that the cutoff graph is a favorable choice for modelling molecular systems since forces and chemical bonds are highly related to interatomic distances.

With notations of the molecular representation, our task formulation is given by:

Task Formulation Considering a biased training dataset consisting of peptide pairs $\mathcal{D} = \{(\mathcal{G}_s, \mathcal{G}_{s+\tau}) | s \in \mathcal{S}\}$, where peptide $\mathcal{G}_{s+\tau}$ is induced from the conventional MD simulation starting from \mathcal{G}_s for a time $\tau \gg \Delta t$, and s represents the simulation time sampled from an arbitrary time set \mathcal{S} . Our goals are: (i) Fit the conditional distribution $\mu(\vec{\mathbf{X}}_{s+\tau} | \vec{\mathbf{X}}_s)$ using a parameterized neural network from \mathcal{D} , denoted as $q_\theta(\vec{\mathbf{X}}_{s+\tau} | \vec{\mathbf{X}}_s)$. (ii) Based on the trained *baseline* model, we aim to train a new parameterized network $p_v(\vec{\mathbf{X}}_{s+\tau} | \vec{\mathbf{X}}_s)$ such that the marginal distributions satisfy $p_v(\vec{\mathbf{X}}) = \frac{1}{Z} q_\theta(\vec{\mathbf{X}}) \exp(-k\varepsilon(\vec{\mathbf{X}}))$, where k and $\varepsilon(\cdot)$ denote the inverse temperature and potential of the molecular system, Z is the partition function to ensure $\int p_v(\vec{\mathbf{X}}) d\vec{\mathbf{X}} = 1$.

4.2 BASELINE BRIDGE MATCHING

We first present a *baseline* generative model $q_\theta(\vec{\mathbf{X}}_{s+\tau} | \vec{\mathbf{X}}_s)$ parameterized by θ to fit the conditional distribution $\mu(\vec{\mathbf{X}}_{s+\tau} | \vec{\mathbf{X}}_s)$ from dataset \mathcal{D} , termed as FBM-BASE. For the sake of convenience and consistency with the continuous diffusion time t , we refer to the conditioned peptide as \mathcal{G}_0 and the target peptide as \mathcal{G}_1 in the following parts.

Bridge Matching Framework Here we leverage the framework of *bridge matching* (Shi et al., 2024) due to the adaptability for arbitrary priors. For a diffusion process in the form of Eq. 1 pinned down at a starting point \mathcal{G}_0 and terminal point \mathcal{G}_1 , it degenerates to a Brownian bridge under the assumption that $f_t = 0$ and $\sigma_t = \sigma$:

$$d\vec{\mathbf{X}}_t = \frac{\vec{\mathbf{X}}_1 - \vec{\mathbf{X}}_t}{1-t} dt + \sigma d\mathbf{B}_t, \quad \vec{\mathbf{X}}_0 = \vec{\mathbf{X}}_0. \quad (3)$$

Denote the conditional distribution of the process as $q_t(\vec{\mathbf{X}}_t | \vec{\mathbf{X}}_0, \vec{\mathbf{X}}_1)$ and its marginal $q_t(\vec{\mathbf{X}}_t)$, the key concept of bridge matching is to find a Markov diffusion with an *vector field* v ,

$$d\vec{\mathbf{Y}}_t = v(\vec{\mathbf{Y}}_t, t) dt + \sigma d\mathbf{B}_t, \quad (4)$$

which admits the same marginal $\vec{\mathbf{Y}}_t \sim q_t$ for $t \in [0, 1]$, thus $\vec{\mathbf{Y}}_1 \sim q_1$. In practice, we use the following regression loss for unbiased estimation:

$$\mathcal{L}_{\text{fwd}} = \mathbb{E}_{t \sim \text{Uni}(0,1), (\mathcal{G}_0, \mathcal{G}_1) \sim \mathcal{D}, \vec{\mathbf{X}}_t \sim q_t(\cdot | \vec{\mathbf{X}}_0, \vec{\mathbf{X}}_1)} \left[\left\| \frac{\vec{\mathbf{X}}_1 - \vec{\mathbf{X}}_t}{1-t} - v(\vec{\mathbf{X}}_t, t) \right\|^2 \right], \quad (5)$$

where $\text{Uni}(0, 1)$ denotes the uniform distribution of $[0, 1]$.

The calculation of Eq. 5 requires sampling from $q_t(\vec{\mathbf{X}}_t | \vec{\mathbf{X}}_0, \vec{\mathbf{X}}_1)$, which usually needs additional SDE simulations. Fortunately, the conditional distribution has a closed-form by solving Eq. 3:

$$q_t(\vec{\mathbf{X}}_t | \vec{\mathbf{X}}_0, \vec{\mathbf{X}}_1) = \mathcal{N}(t\vec{\mathbf{X}}_1 + (1-t)\vec{\mathbf{X}}_0, t(1-t)\sigma^2 \mathbf{I}), \quad (6)$$

where we can sample $\vec{\mathbf{X}}_t$ efficiently during each training step with any given t .

Linkage between Vector Field and Score We further investigate the relation between the vector field v_t and the marginal score function $\nabla \log q_t$, since the latter has deeper connections to the marginal distribution q_t that we are interested in.

Given $\mathcal{G}_0, \mathcal{G}_1$, we define the conditional score function $s_t(\vec{\mathbf{X}}_t | \vec{\mathbf{X}}_0, \vec{\mathbf{X}}_1) = \nabla \log q_t(\vec{\mathbf{X}}_t | \vec{\mathbf{X}}_0, \vec{\mathbf{X}}_1)$. Based on Eq. 6, the closed-form of s_t is given by:

$$s_t(\vec{\mathbf{X}}_t | \vec{\mathbf{X}}_0, \vec{\mathbf{X}}_1) = -\frac{\vec{\mathbf{X}}_t - [t\vec{\mathbf{X}}_1 + (1-t)\vec{\mathbf{X}}_0]}{t(1-t)\sigma^2} = \frac{1}{\sigma^2} \left[\frac{\vec{\mathbf{X}}_1 - \vec{\mathbf{X}}_t}{1-t} - \frac{\vec{\mathbf{X}}_t - \vec{\mathbf{X}}_0}{t} \right]. \quad (7)$$

It is noted that the first term of Eq. 7 has the same form as in the training objective of Eq. 5. According to Anderson (1982), interestingly we find that the second term is exactly the drift term of the reverse-time diffusion process of Eq. 3:

$$d\vec{\mathbf{X}}_t = \frac{\vec{\mathbf{X}}_t - \vec{\mathbf{X}}_0}{t} dt + \sigma d\mathbf{B}_t, \quad \vec{\mathbf{X}}_1 = \vec{\mathbf{X}}_1. \quad (8)$$

Similar to Eq. 5, we introduce another network u to imitate the reverse-time diffusion process:

$$\mathcal{L}_{\text{rev}} = \mathbb{E}_{t \sim \text{Uni}(0,1), (\mathcal{G}_0, \mathcal{G}_1) \sim \mathcal{D}, \vec{\mathbf{X}}_t \sim q_t(\cdot | \vec{\mathbf{X}}_0, \vec{\mathbf{X}}_1)} [|| \frac{\vec{\mathbf{X}}_t - \vec{\mathbf{X}}_0}{t} - u(\vec{\mathbf{X}}_t, t) ||^2]. \quad (9)$$

From Eq. 5 and Eq. 9, it can be verified that the expectations of vector fields are given by:

$$v^*(\vec{\mathbf{X}}_t, t) = \mathbb{E}_{\vec{\mathbf{X}}_0, \vec{\mathbf{X}}_1 \sim q_t(\cdot, \cdot | \vec{\mathbf{X}}_t)} [\frac{\vec{\mathbf{X}}_1 - \vec{\mathbf{X}}_0}{1-t}], \quad u^*(\vec{\mathbf{X}}_t, t) = \mathbb{E}_{\vec{\mathbf{X}}_0, \vec{\mathbf{X}}_1 \sim q_t(\cdot, \cdot | \vec{\mathbf{X}}_t)} [\frac{\vec{\mathbf{X}}_t - \vec{\mathbf{X}}_0}{t}]. \quad (10)$$

Based on Eq. 7, we define the marginal score as follows:

$$s_t^*(\vec{\mathbf{X}}_t) = \mathbb{E}_{\vec{\mathbf{X}}_0, \vec{\mathbf{X}}_1 \sim q_t(\cdot, \cdot | \vec{\mathbf{X}}_t)} [s_t(\vec{\mathbf{X}}_t | \vec{\mathbf{X}}_0, \vec{\mathbf{X}}_1)] = \frac{v^*(\vec{\mathbf{X}}_t, t) - u^*(\vec{\mathbf{X}}_t, t)}{\sigma^2}. \quad (11)$$

Then Prop. 4.1 reveals the equivalence relation between s_t^* and the marginal score $\nabla \log q_t$:

Proposition 4.1. *Given q_t the marginal distribution of the Brownian bridge 3 at diffusion time t and s_t^* described in Eq. 11, then $s_t^* = \nabla \log q_t$ holds.*

Full Loss In addition to the aforementioned regression losses, we introduce an auxiliary loss from Yim et al. (2023) which promotes better predictions of pairwise atomic relations. The loss is defined as:

$$\mathcal{L}_{\text{aux}} = (1-t) \cdot \frac{||\mathbf{1}_{D_0 < 6\text{\AA}}(D_0 - \hat{D}_0)||^2}{\sum \mathbf{1}_{D_0 < 6\text{\AA}} - N} + t \cdot \frac{||\mathbf{1}_{D_1 < 6\text{\AA}}(D_1 - \hat{D}_1)||^2}{\sum \mathbf{1}_{D_1 < 6\text{\AA}} - N}, \quad (12)$$

where $D_0, D_1 \in \mathbb{R}^{N \times N}$ denote pairwise distances between all atoms of peptide \mathcal{G}_0 and \mathcal{G}_1 , and \hat{D}_0, \hat{D}_1 are defined in the same way based on the estimated starting point $\hat{\vec{\mathbf{X}}}_0 = \vec{\mathbf{X}}_t - t u(\vec{\mathbf{X}}_t, t)$ and terminal point $\hat{\vec{\mathbf{X}}}_1 = \vec{\mathbf{X}}_t + (1-t)v(\vec{\mathbf{X}}_t, t)$. The full loss is given by:

$$\mathcal{L}_{\text{base}} = \mathcal{L}_{\text{fwd}} + \mathcal{L}_{\text{rev}} + \lambda_{\text{aux}} \cdot \mathcal{L}_{\text{aux}}, \quad (13)$$

where λ_{aux} is a hyperparameter to balance the weight of different training objectives.

4.3 FORCE-GUIDED BRIDGE MATCHING

In most cases, the training datasets are biased from the target distribution (e.g., the Boltzmann distribution), which leads to inevitable prediction bias even for superior generative models. Inspired by Wang et al. (2024), we incorporate an *intermediate force field* into the bridge matching framework, aiming to target at a Boltzmann-like distribution, denoted $p_1(\vec{\mathbf{X}}) = \frac{1}{Z} q_1(\vec{\mathbf{X}}) \exp(-k\varepsilon(\vec{\mathbf{X}}))$. The overall framework of FBM as well as FBM-BASE is demonstrated in Figure 2.

Intermediate Force Field To integrate the bridge matching generative framework, our key idea is to construct a new probabilistic path p_t based on the existing probabilistic path q_t such that the following condition is satisfied for $t \in [0, 1]$:

$$p_t(\vec{\mathbf{X}}_t) = \frac{1}{Z_t} q_t(\vec{\mathbf{X}}_t) \exp(-k\varepsilon_t(\vec{\mathbf{X}}_t)), \quad \varepsilon_0 = \varepsilon_1 = \varepsilon. \quad (14)$$

Here Z_t is the partition function and ε_t is an artificially designed *intermediate potential* of the process, which should converge to the real potential function ε when $t \rightarrow 0^+$ and $t \rightarrow 1^-$ for consistency.

Further, given the starting and terminal point $(\mathcal{G}_0, \mathcal{G}_1)$, we assume $p_t(\vec{\mathbf{X}}_t | \vec{\mathbf{X}}_0, \vec{\mathbf{X}}_1) = q_t(\vec{\mathbf{X}}_t | \vec{\mathbf{X}}_0, \vec{\mathbf{X}}_1)$ as in Eq. 6, thereby the stochastic process governed by p_t shares the same form with Eq. 3. Then the intermediate potential ε_t and correspondingly, the intermediate force field $\nabla \varepsilon_t$ are given in Prop. 4.2:

Proposition 4.2. *Assume that τ is sufficiently large, such that the random variables $\vec{\mathbf{X}}_0$ and $\vec{\mathbf{X}}_1$ following the densities q_0, q_1 and p_0, p_1 are both independent, then the intermediate potential ε_t and the intermediate force field $\nabla \varepsilon_t$ are given by:*

$$\varepsilon_t(\vec{\mathbf{X}}_t) = -\frac{1}{k} \log \mathbb{E}_{q_t(\vec{\mathbf{X}}_0, \vec{\mathbf{X}}_1 | \vec{\mathbf{X}}_t)} [\exp(-k(\varepsilon(\vec{\mathbf{X}}_0) + \varepsilon(\vec{\mathbf{X}}_1)))] + \frac{1}{k} \log \frac{Z_0 Z_1}{Z_t}, \quad (15)$$

$$\nabla \varepsilon_t(\vec{\mathbf{X}}_t) = \frac{\mathbb{E}_{q_t(\vec{\mathbf{X}}_0, \vec{\mathbf{X}}_1)} [q_t(\vec{\mathbf{X}}_t | \vec{\mathbf{X}}_0, \vec{\mathbf{X}}_1) \exp(-k(\varepsilon(\vec{\mathbf{X}}_0) + \varepsilon(\vec{\mathbf{X}}_1))) \zeta(\vec{\mathbf{X}}_0, \vec{\mathbf{X}}_1, \vec{\mathbf{X}}_t)]}{k \mathbb{E}_{q_t(\vec{\mathbf{X}}_0, \vec{\mathbf{X}}_1)} [q_t(\vec{\mathbf{X}}_t | \vec{\mathbf{X}}_0, \vec{\mathbf{X}}_1) \exp(-k(\varepsilon(\vec{\mathbf{X}}_0) + \varepsilon(\vec{\mathbf{X}}_1)))]}. \quad (16)$$

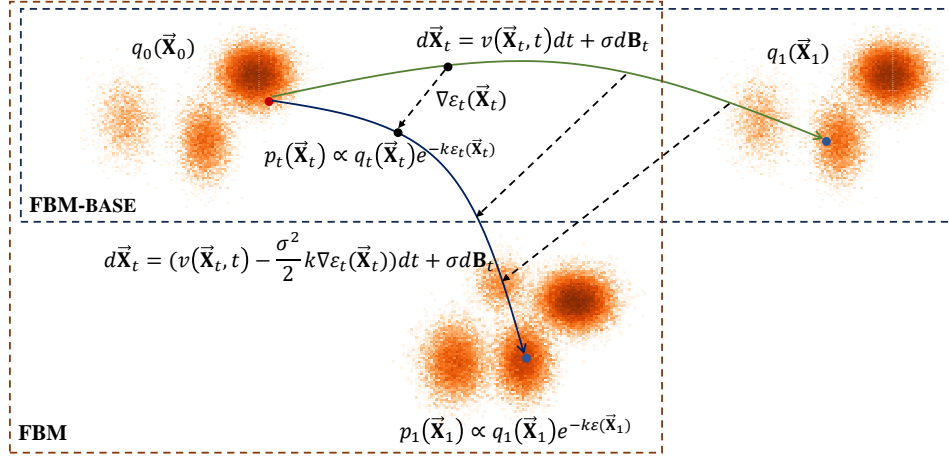


Figure 2: The overall framework of FBM-BASE and FBM. **A.** Firstly, FBM-BASE leverages the bridge matching framework to learn time-coarsened dynamics on a dataset with prior distribution q_0 and target distribution q_1 , which are mostly biased from the underlying Boltzmann distribution. **B.** With the guidance of an intermediate force field $\nabla \varepsilon_t$ at diffusion time t , the marginal distribution admits $p_t(\vec{X}_t) \propto q_t(\vec{X}_t) \exp(-k\varepsilon_t(\vec{X}_t))$, thereby the target distribution of FBM is debiased to a Boltzmann-like distribution p_1 .

Here we denote $\zeta(\vec{X}_0, \vec{X}_1, \vec{X}_t) = \nabla \log q_t(\vec{X}_t) - \nabla \log q_t(\vec{X}_t | \vec{X}_0, \vec{X}_1)$ for brevity, where s_t^* is an unbiased estimation of the first term based on Prop. 4.1 and the second term has a closed-form solution according to Eq. 7. For the denominator term of Eq. 16, we estimate the expectation with samples in a mini-batch during training instead of computing over the entire data distribution (Lu et al., 2023a). We hope to use a network w to imitate the intermediate force field with the following training objective:

$$\mathcal{L}_{\text{iff}} = \mathbb{E}_{t, (\mathcal{G}_0, \mathcal{G}_1), q_t(\cdot | \vec{X}_0, \vec{X}_1)} \left[\left\| \frac{\exp(-k(\varepsilon(\vec{X}_0) + \varepsilon(\vec{X}_1))) \zeta(\vec{X}_0, \vec{X}_1, \vec{X}_t)}{k \mathbb{E}_{q(\vec{X}_0, \vec{X}_1)^B} [q_t(\vec{X}_t | \vec{X}_0, \vec{X}_1) \exp(-k(\varepsilon(\vec{X}_0) + \varepsilon(\vec{X}_1)))]} - w(\vec{X}_t, t) \right\|^2 \right], \quad (17)$$

where B denotes the mini-batch size of each training step.

Empirically, large variances are noticed during training when t is close to 0 and 1. Note that the intermediate force field converges to the MD force field $\nabla \varepsilon$ at $t = 0, 1$, which is guaranteed by Prop. 4.3:

Proposition 4.3. *Given $\varepsilon_0 = \varepsilon_1 = \varepsilon$ and the intermediate force field described in Eq. 16, the continuity condition $\lim_{t \rightarrow 0^+} \nabla \varepsilon_t(\vec{X}_t) = \nabla \varepsilon(\vec{X}_0)$, $\lim_{t \rightarrow 1^-} \nabla \varepsilon_t(\vec{X}_t) = \nabla \varepsilon(\vec{X}_1)$ holds.*

Therefore, we leverage two additional networks α, β to learn boundary MD force fields:

$$\mathcal{L}_{\text{bnd}} = \mathbb{E}_{t, (\mathcal{G}_0, \mathcal{G}_1), q_t(\cdot | \vec{X}_0, \vec{X}_1)} [\|\nabla \varepsilon(\vec{X}_0) - \alpha(\vec{X}_t, t)\|^2 + \|\nabla \varepsilon(\vec{X}_1) - \beta(\vec{X}_t, t)\|^2], \quad (18)$$

and we construct the network w_t in the interpolation form similar to Máté & Fleuret (2023), with γ another parameterized network: $w(\vec{X}_t, t) = (1-t)\alpha(\vec{X}_t, t) + t\beta(\vec{X}_t, t) + t(1-t)\gamma(\vec{X}_t, t)$. Then the ultimate loss for training our FBM is given by:

$$\mathcal{L}_{\text{FBM}} = \mathcal{L}_{\text{iff}} + \mathcal{L}_{\text{bnd}}. \quad (19)$$

Force-guided Inference After obtaining the estimation of $\nabla \varepsilon_t$ with network w , the issue remained is how to transform the intermediate force field into the vector field representation so that the inference can be performed in the way consistent with Eq. 4. Denote $v'(\vec{X}_t, t)$ as the vector field that generates the probability path p_t , Prop. 4.4 provides an unbiased estimation of $v'(\vec{X}_t, t)$ in terms of the vector field expectation of the baseline model $v^*(\vec{X}_t, t)$ and the intermediate force field $\nabla \varepsilon_t$:

Proposition 4.4. *Given the prerequisites in Prop. 4.2, we have $v'(\vec{X}_t, t) = v^*(\vec{X}_t, t) - \frac{\sigma^2}{2} k \nabla \varepsilon_t(\vec{X}_t)$ under some mild assumptions.*

Additional details and pseudo codes for training and inference with our FBM-BASE and FBM are shown in § D.

5 EXPERIMENTS

5.1 EXPERIMENTAL SETUP

Dataset Generation We evaluate FBM on small peptide systems, which exhibit certain regularities in their sequences and structures. Firstly, we screen valid peptides between 3-10 residues from the sequence data¹ provided by PDB (Berman et al., 2000). Next, we perform data cleaning according to the following criterion: each peptide must contain only the 20 natural amino acids, and the number of any type of residue should not exceed 50% of the sequence length. We then cluster the data with a sequence identity threshold of 60% by MMseq2 (Steinegger & Söding, 2017), and randomly sample one peptide from each cluster to obtain a non-redundant dataset. Considering the computing resource constraints, we randomly select 136/14 peptides for the training/test set respectively. The structures of all 150 peptides are predicted by open-source tools RDKit and PDBfixer, which are sent as initial states to generate MD trajectories using OpenMM (Eastman et al., 2017) afterwards. Finally, the peptide pairs for training are then sampled from trajectories in the way depicted in § 4.1. The MD simulation setups and the statistical details of our curated dataset, named as PepMD, are both illustrated in § E.1. Moreover, we also investigate Alanine-Dipeptide (AD), a simple peptide with only 22 atoms that is commonly studied for MD benchmark. The initial structure and reference MD trajectories of AD are all obtained from mdshare² without post-processing.

Baselines We compare our FBM with the following generative models that learn time-coarsened dynamics: (i) Timewarp (Klein et al., 2024), the current state-of-the-art model targeting the Boltzmann distribution by MCMC resampling, which exhibits superior transferability to unseen peptide systems. (ii) ITO (Schreiner et al., 2024), a conditional diffusion model that learns multiple time-resolution dynamics. (iii) Score Dynamics (Hsu et al., 2024), a score-based diffusion model that learns discrete transitions of the dynamic variables. All models are trained on PepMD from scratch for fair comparison.

Metrics Following Wang et al. (2024), we evaluate generated conformation ensembles against the full MD trajectories as to their validity, flexibility, and distributional similarity. We provide brief descriptions of the metrics in this part and further details are illustrated in § E.2:

- **Validity.** We regard a molecular conformation as *valid* when it is governed by certain physical constraints. Following Lu et al. (2023b), we judge whether a conformation is valid by the criterion: no bond clashes between any residue pairs and no bond breaks between adjacent residues, based on coordinates of α -carbons. The corresponding metric, named as VAL-CA, represents the fraction of valid conformations in the full generated ensembles.
- **Flexibility.** The generated structures are further required to exhibit flexibility to capture dynamic characteristics. Following Janson et al. (2023), we report the root mean square error of contact maps between generated ensembles and reference MD trajectories as a measure of *flexibility*, termed as CONTACT.
- **Distributional similarity.** We focus on the similarity between the distribution generated by the model and the target Boltzmann distribution as well. Instead of the costly computation of the Boltzmann density, we project the molecular conformations onto following low-dimensional feature spaces and calculate the Jensen-Shannon (JS) distance as a substitute (Lu et al., 2023b): (i) pairwise distances between α -carbons of residues (PWD); (ii) radius-of-gyration (RG) that measures the distribution of α -carbons to the center-of-mass; (iii) the *time-lagged independent components* (Pérez-Hernández et al., 2013) (TIC) based on dihedrals and pairwise distances of α -carbons, where only the slowest components, TIC 0 and TIC 1, are taken into consideration. For each metric, the mean JS distance along all feature dimensions are reported.

¹https://files.wwpdb.org/pub/pdb/derived_data/pdb_seqres.txt.gz.

²<https://github.com/markovmodel/mdshare>.

5.2 METASTABLE STATES EXPLORATION FOR AD

We first investigate how well the generated ensembles can travel across different metastable states of AD. Due to the simple structure of AD with only one peptide bond, some metrics are not applicable and here we use TIC and TIC-2D (*i.e.*, the joint distribution of TIC 0 and TIC 1) as the measures of distributional similarity. In particular, the backbone dihedrals of AD, psi and phi, are considered the most challenging variables for state transitions. Therefore, we include the similarity measurement of the joint distribution of psi-phi, *i.e.* the *Ramachandran plot* (Ramachandran et al., 1963), denoted as RAM.

In Table 1 we provide evaluation results on AD, where models sample new states from the same initial state for a chain length of 10^4 , and we adopt Algorithm 3 for inference with FBM-BASE and FBM. It reveals that the generated ensembles with FBM show close agreement with MD trajectories, especially on the slowest transition variables psi and phi. Moreover, FBM exhibits promoted generative ability with force guidance compared to FBM-BASE. In Figure 3 we illustrate Ramachandran plots of alanine dipeptide with generated ensembles of models, where three known metastable states are labeled in order. We find that ITO and Score Dynamics (SD) probably ignore reasonable regions of conformations during sampling, and Timewarp shows explicit clusters yet deviates from real metastable regions. In contrast, both FBM-BASE and FBM visit all three metastable states, while FBM concentrates more on clusters with higher density (region 2,3) with less invalid conformations generated, which aligns with our expectation of force guidance.

Table 1: Results on alanine dipeptide. Values are averaged over 3 independent runs with random seeds. The best result for each metric is shown in **bold** and the second best is underlined.

MODELS	JS DISTANCE (\downarrow)		
	RAM	TIC	TIC-2D
TIMEWARP	0.737	<u>0.520</u>	0.707
ITO	0.680	0.551	0.772
SCORE DYNAMICS	0.704	0.612	0.799
FBM-BASE	<u>0.663</u>	0.527	<u>0.691</u>
FBM	0.644	0.516	0.689

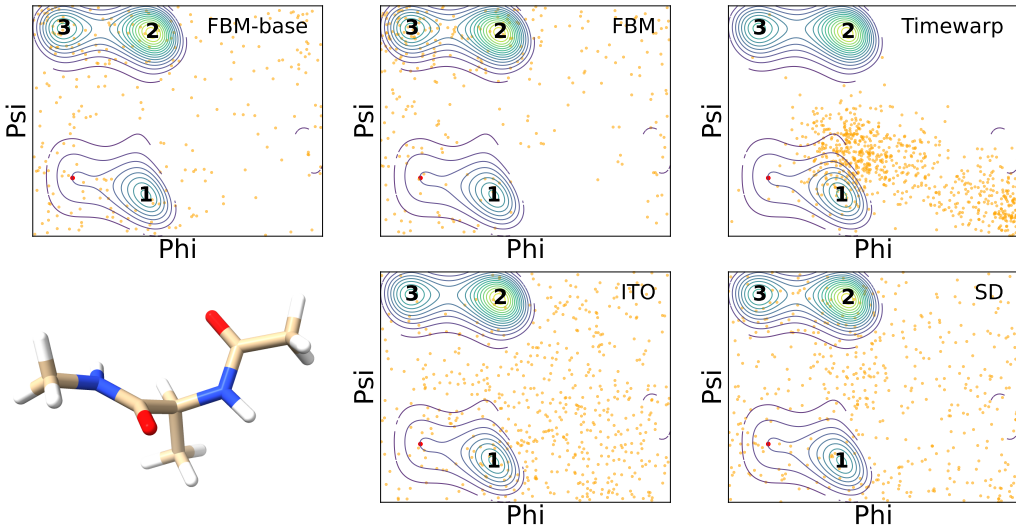


Figure 3: Ramachandran plots of alanine dipeptide with generated ensembles of models. The initial state is indicated with the red cross. Contours represent the kernel densities estimated by the MD trajectory and the generated conformations are shown in scatter.

5.3 TRANSFERABILITY TO UNSEEN PEPTIDES OF PEPMD

We then explore the transferability of models to unseen peptides with various sequence lengths of PepMD. We use all metrics in § 5.1 for evaluation and the results on 14 test peptides of PepMD are demonstrated in Table 2, where all samples are generated for a chain length of 10^3 . Timewarp achieves the best result on TIC-2D, yet at the cost of much less valid samples. Our models, FBM-BASE and FBM, showcase superiority over flexibility, distributional similarity and especially validity of conformation ensembles. Moreover, under force guidance, the generated ensembles are more akin to the Boltzmann distribution while maintaining reasonable conformations.

Table 2: Results on the test set of PepMD. Values are shown in median/std of all 14 test peptides in a single run. The best result for each metric is shown in **bold** and the second best is underlined.

MODELS	JS DISTANCE (\downarrow)				VAL-CA (\uparrow)	CONTACT (\downarrow)
	PWD	RG	TIC	TIC-2D		
TIMEWARP	0.641/0.095	0.693/0.100	0.656/0.090	0.795/0.037	0.292/0.220	0.266/0.140
ITO	0.833/0.000	0.829/0.012	0.789/0.067	0.833/0.000	0.001/0.000	0.940/0.081
SD	0.823/0.030	0.818/0.041	0.773/0.032	0.832/0.001	0.006/0.016	0.824/0.095
FBM-BASE	<u>0.583/0.070</u>	<u>0.576/0.134</u>	<u>0.641/0.071</u>	0.809/0.025	<u>0.691/0.182</u>	<u>0.216/0.140</u>
FBM	0.573/0.067	0.533/0.156	0.635/0.072	<u>0.798/0.034</u>	0.798/0.135	0.192/0.137

In Figure 5 we provide further case study on the test peptide 1e28:C (*i.e.*, chain C of PDB 1e28) with 8 residues and 3 major metastable states. For such complex peptide, ITO and Score Dynamics even hardly sample in high-density regions. The generated samples of Timewarp are mainly concentrated in region 2, but scarcely access region 1 as well as region 3 with the highest density, indicating a lack of transferability in this peptide. The most appealing part is, given both FBM and FBM-BASE have accessed all three metastable states, the intermediate force field accurately guides the generation from region 1 to the higher-density region 3 with the correct relative weights, while also reducing the likelihood of generating invalid conformations. Moreover, we compare the reference structures and generated conformations with FBM of three metastable states based on their Root-Mean-Square-Deviation (RMSD) in Figure 4, where each sample is the nearest to the corresponding cluster center among the conformation ensembles (Wang et al., 2024). FBM shows an accurate recovery of known, representative conformations with a much shorter sampling path. Therefore, we believe that FBM demonstrates exceptional performance on transferability to small peptide systems compared to all baselines.

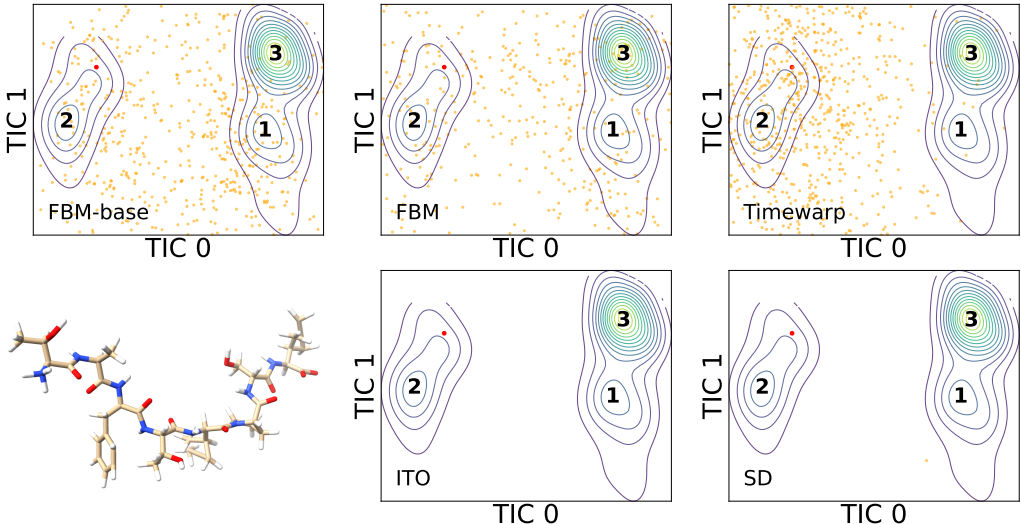


Figure 4: TIC plots of peptide 1e28:C with generated ensembles of models.

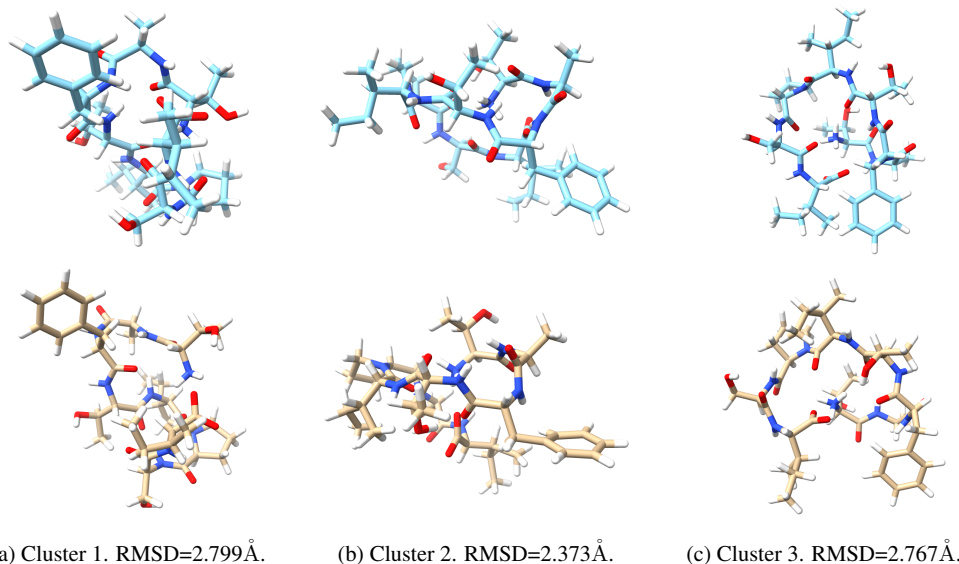


Figure 5: Comparison between generated structures with FBM (yellow) and reference structures of MD trajectories (blue) for three metastable states of peptide 1e28:C.

6 CONCLUSION AND FUTURE WORK

In this work, we present a novel generative model FBM for time-coarsened dynamics in a full-atom fashion. We first leverage the bridge matching framework to construct the baseline model FBM-BASE for learning dynamics on arbitrary training dataset. Based on FBM-BASE, we further incorporate an intermediate force field to the framework for external physical guidance, which is theoretically guaranteed to target the Boltzmann-like distribution from biased data distributions. Experiments on alanine dipeptide and our curated dataset PepMD showcase superiority of generated ensembles with FBM on comprehensive metrics and demonstrate transferability to unseen peptide systems as well.

As the first attempt to introduce physical priors into bridge matching for time-coarsened dynamics, our method has considerable room for improvement. Firstly, our experiments have been conducted on small peptides with fewer than 10 residues. Further exploration on more complex molecular systems (e.g., proteins with much longer sequences) is warranted. Secondly, we utilize the marginal distribution of the baseline model rather than directly targeting the underlying Boltzmann distribution, which leaves room for theoretical advancement. Lastly, FBM seems unable to avoid sampling unreasonable conformations during transitions between metastable states, where methods for rapid and jump-like state transition are of great importance.

REFERENCES

- Brian DO Anderson. Reverse-time diffusion equation models. *Stochastic Processes and their Applications*, 12(3):313–326, 1982.
- Jimmy Lei Ba, Jamie Ryan Kiros, and Geoffrey E Hinton. Layer normalization. *arXiv preprint arXiv:1607.06450*, 2016.
- Helen M Berman, John Westbrook, Zukang Feng, Gary Gilliland, Talapady N Bhat, Helge Weissig, Ilya N Shindyalov, and Philip E Bourne. The protein data bank. *Nucleic acids research*, 28(1): 235–242, 2000.
- Xin Dong, Shangyu Chen, and Sinno Pan. Learning to prune deep neural networks via layer-wise optimal brain surgeon. *Advances in neural information processing systems*, 30, 2017.
- Jacob D Durrant and J Andrew McCammon. Molecular dynamics simulations and drug discovery. *BMC biology*, 9:1–9, 2011.

- Peter Eastman, Jason Swails, John D Chodera, Robert T McGibbon, Yutong Zhao, Kyle A Beauchamp, Lee-Ping Wang, Andrew C Simmonett, Matthew P Harrigan, Chaya D Stern, et al. Openmm 7: Rapid development of high performance algorithms for molecular dynamics. *PLoS computational biology*, 13(7):e1005659, 2017.
- Sebastian Falkner, Alessandro Coretti, Salvatore Romano, Phillip L Geissler, and Christoph Dellago. Conditioning boltzmann generators for rare event sampling. *Machine Learning: Science and Technology*, 4(3):035050, 2023.
- Xiang Fu, Tian Xie, Nathan J Rebello, Bradley Olsen, and Tommi S Jaakkola. Simulate time-integrated coarse-grained molecular dynamics with multi-scale graph networks. *Transactions on Machine Learning Research*, 2023.
- Moritz Hoffmann, Martin Scherer, Tim Hempel, Andreas Mardt, Brian de Silva, Brooke E Husic, Stefan Klus, Hao Wu, Nathan Kutz, Steven L Brunton, et al. Deeptime: a python library for machine learning dynamical models from time series data. *Machine Learning: Science and Technology*, 3(1):015009, 2021.
- Tim Hsu, Babak Sadigh, Vasily Bulatov, and Fei Zhou. Score dynamics: Scaling molecular dynamics with picoseconds time steps via conditional diffusion model. *Journal of Chemical Theory and Computation*, 20(6):2335–2348, 2024.
- Giacomo Janson, Gilberto Valdes-Garcia, Lim Heo, and Michael Feig. Direct generation of protein conformational ensembles via machine learning. *Nature Communications*, 14(1):774, 2023.
- Leon Klein and Frank Noé. Transferable boltzmann generators. *arXiv preprint arXiv:2406.14426*, 2024.
- Leon Klein, Andrew Foong, Tor Fjelde, Bruno Mlodozieniec, Marc Brockschmidt, Sebastian Nowozin, Frank Noé, and Ryota Tomioka. Timewarp: Transferable acceleration of molecular dynamics by learning time-coarsened dynamics. *Advances in Neural Information Processing Systems*, 36, 2024.
- Jonas Köhler, Andreas Krämer, and Frank Noé. Smooth normalizing flows. *Advances in Neural Information Processing Systems*, 34:2796–2809, 2021.
- Jonas Köhler, Michele Invernizzi, Pim De Haan, and Frank Noé. Rigid body flows for sampling molecular crystal structures. In *International Conference on Machine Learning*, pp. 17301–17326. PMLR, 2023.
- Alessandro Laio and Michele Parrinello. Escaping free-energy minima. *Proceedings of the national academy of sciences*, 99(20):12562–12566, 2002.
- Kresten Lindorff-Larsen, Stefano Piana, Ron O Dror, and David E Shaw. How fast-folding proteins fold. *Science*, 334(6055):517–520, 2011.
- Cheng Lu, Huayu Chen, Jianfei Chen, Hang Su, Chongxuan Li, and Jun Zhu. Contrastive energy prediction for exact energy-guided diffusion sampling in offline reinforcement learning. In *International Conference on Machine Learning*, pp. 22825–22855. PMLR, 2023a.
- Jiarui Lu, Bozita Zhong, Zuobai Zhang, and Jian Tang. Str2str: A score-based framework for zero-shot protein conformation sampling. *arXiv preprint arXiv:2306.03117*, 2023b.
- Bálint Máté and François Fleuret. Learning interpolations between boltzmann densities. *arXiv preprint arXiv:2301.07388*, 2023.
- Nicholas Metropolis, Arianna W Rosenbluth, Marshall N Rosenbluth, Augusta H Teller, and Edward Teller. Equation of state calculations by fast computing machines. *The journal of chemical physics*, 21(6):1087–1092, 1953.
- Erik C Neyts and Annemie Bogaerts. Combining molecular dynamics with monte carlo simulations: implementations and applications. *Theoretical Chemistry in Belgium: A Topical Collection from Theoretical Chemistry Accounts*, pp. 277–288, 2014.

- Frank Noé, Simon Olsson, Jonas Köhler, and Hao Wu. Boltzmann generators: Sampling equilibrium states of many-body systems with deep learning. *Science*, 365(6457):eaaw1147, 2019.
- Yui Tik Pang, Yinglong Miao, Yi Wang, and J Andrew McCammon. Gaussian accelerated molecular dynamics in namd. *Journal of chemical theory and computation*, 13(1):9–19, 2017.
- David A Pearlman, David A Case, James W Caldwell, Wilson S Ross, Thomas E Cheatham III, Steve DeBolt, David Ferguson, George Seibel, and Peter Kollman. Amber, a package of computer programs for applying molecular mechanics, normal mode analysis, molecular dynamics and free energy calculations to simulate the structural and energetic properties of molecules. *Computer Physics Communications*, 91(1-3):1–41, 1995.
- Raul P. Pelaez, Guillem Simeon, Raimondas Galvelis, Antonio Mirarchi, Peter Eastman, Stefan Doerr, Philipp Thölke, Thomas E. Markland, and Gianni De Fabritiis. Torchmd-net 2.0: Fast neural network potentials for molecular simulations, 2024.
- Guillermo Pérez-Hernández, Fabian Paul, Toni Giorgino, Gianni De Fabritiis, and Frank Noé. Identification of slow molecular order parameters for markov model construction. *The Journal of chemical physics*, 139(1), 2013.
- G.N. Ramachandran, C. Ramakrishnan, and V. Sasisekharan. Stereochemistry of polypeptide chain configurations.“. *J. mol. Biol*, 7:95–99, 1963.
- L Chris G Rogers and David Williams. *Diffusions, Markov processes, and martingales: Itô calculus*, volume 2. Cambridge university press, 2000.
- Babak Sadigh, Paul Erhart, Alexander Stukowski, Alfredo Caro, Enrique Martinez, and Luis Zepeda-Ruiz. Scalable parallel monte carlo algorithm for atomistic simulations of precipitation in alloys. *Physical Review B—Condensed Matter and Materials Physics*, 85(18):184203, 2012.
- Outi MH Salo-Ahen, Ida Alanko, Rajendra Bhadane, Alexandre MJJ Bonvin, Rodrigo Vargas Honorato, Shakhawath Hossain, André H Juffer, Aleksei Kabedev, Maija Lahtela-Kakkonen, Anders Støttrup Larsen, et al. Molecular dynamics simulations in drug discovery and pharmaceutical development. *Processes*, 9(1):71, 2020.
- Mathias Schreiner, Ole Winther, and Simon Olsson. Implicit transfer operator learning: Multiple time-resolution models for molecular dynamics. *Advances in Neural Information Processing Systems*, 36, 2024.
- Yuyang Shi, Valentin De Bortoli, Andrew Campbell, and Arnaud Doucet. Diffusion schrödinger bridge matching. *Advances in Neural Information Processing Systems*, 36, 2024.
- Martin Steinegger and Johannes Söding. Mmseqs2 enables sensitive protein sequence searching for the analysis of massive data sets. *Nature biotechnology*, 35(11):1026–1028, 2017.
- Yuji Sugita and Yuko Okamoto. Replica-exchange molecular dynamics method for protein folding. *Chemical physics letters*, 314(1-2):141–151, 1999.
- Philipp Thölke and Gianni De Fabritiis. Equivariant transformers for neural network based molecular potentials. In *International Conference on Learning Representations*, 2022. URL <https://openreview.net/forum?id=zNHZqZ9wrRB>.
- Kenno Vanommeslaeghe, Elizabeth Hatcher, Chayan Acharya, Sibsankar Kundu, Shijun Zhong, Jihyun Shim, Eva Darian, Olgun Guvench, P Lopes, Igor Vorobyov, et al. Charmm general force field: A force field for drug-like molecules compatible with the charmm all-atom additive biological force fields. *Journal of computational chemistry*, 31(4):671–690, 2010.
- Arthur F Voter et al. Temperature-accelerated dynamics for simulation of infrequent events. *The Journal of Chemical Physics*, 112(21):9599–9606, 2000.
- Debby D Wang, Le Ou-Yang, Haoran Xie, Mengxu Zhu, and Hong Yan. Predicting the impacts of mutations on protein-ligand binding affinity based on molecular dynamics simulations and machine learning methods. *Computational and structural biotechnology journal*, 18:439–454, 2020.

Yan Wang, Lihao Wang, Yuning Shen, Yiqun Wang, Huizhuo Yuan, Yue Wu, and Quanquan Gu. Protein conformation generation via force-guided se (3) diffusion models. *arXiv preprint arXiv:2403.14088*, 2024.

D Wolf, V Yamakov, SR Phillpot, A Mukherjee, and H Gleiter. Deformation of nanocrystalline materials by molecular-dynamics simulation: relationship to experiments? *Acta Materialia*, 53 (1):1–40, 2005.

Jason Yim, Brian L Trippe, Valentin De Bortoli, Emile Mathieu, Arnaud Doucet, Regina Barzilay, and Tommi Jaakkola. Se (3) diffusion model with application to protein backbone generation. *arXiv preprint arXiv:2302.02277*, 2023.

APPENDIX

A REPRODUCIBILITY

Our source code and the curated dataset PepMD are all available at <https://github.com/yaledeus/FBM>.

B PROOFS OF PROPOSITIONS

Proof of Proposition 4.1. From the definition of s_t^* in Eq. 11, the following equation holds:

$$s_t^*(\vec{\mathbf{X}}_t) = \mathbb{E}_{\vec{\mathbf{X}}_0, \vec{\mathbf{X}}_1 \sim q_t(\cdot, \cdot | \vec{\mathbf{X}}_t)} [\nabla \log q_t(\vec{\mathbf{X}}_t | \vec{\mathbf{X}}_0, \vec{\mathbf{X}}_1)] \quad (20)$$

$$= \iint \nabla \log q_t(\vec{\mathbf{X}}_t | \vec{\mathbf{X}}_0, \vec{\mathbf{X}}_1) q_t(\vec{\mathbf{X}}_0, \vec{\mathbf{X}}_1 | \vec{\mathbf{X}}_t) d\vec{\mathbf{X}}_0 d\vec{\mathbf{X}}_1 \quad (21)$$

$$= \frac{1}{q_t(\vec{\mathbf{X}}_t)} \iint \nabla q_t(\vec{\mathbf{X}}_t | \vec{\mathbf{X}}_0, \vec{\mathbf{X}}_1) q(\vec{\mathbf{X}}_0, \vec{\mathbf{X}}_1) d\vec{\mathbf{X}}_0 d\vec{\mathbf{X}}_1 \quad (22)$$

$$= \frac{1}{q_t(\vec{\mathbf{X}}_t)} \nabla \iint q_t(\vec{\mathbf{X}}_t | \vec{\mathbf{X}}_0, \vec{\mathbf{X}}_1) q(\vec{\mathbf{X}}_0, \vec{\mathbf{X}}_1) d\vec{\mathbf{X}}_0 d\vec{\mathbf{X}}_1 \quad (23)$$

$$= \frac{\nabla q_t(\vec{\mathbf{X}}_t)}{q_t(\vec{\mathbf{X}}_t)} = \nabla \log q_t(\vec{\mathbf{X}}_t), \quad (24)$$

where in the second equality we use the Bayesian rule of probability, $q(\vec{\mathbf{X}}_0, \vec{\mathbf{X}}_1)$ denotes the joint distribution of random variables $\vec{\mathbf{X}}_0, \vec{\mathbf{X}}_1$ under the probability path q_t . Furthermore, the third equality is justified by assuming the integrands satisfy the regularity conditions of the Leibniz Rule. \square

Proof of Proposition 4.2. Given the random variables $\vec{\mathbf{X}}_0$ and $\vec{\mathbf{X}}_1$ following the densities q_0, q_1 and p_0, p_1 are both independent, the joint distributions of $\vec{\mathbf{X}}_0, \vec{\mathbf{X}}_1$ under two probability paths, termed as $q(\vec{\mathbf{X}}_0, \vec{\mathbf{X}}_1)$ and $p(\vec{\mathbf{X}}_0, \vec{\mathbf{X}}_1)$, satisfy:

$$p(\vec{\mathbf{X}}_0, \vec{\mathbf{X}}_1) = p_0(\vec{\mathbf{X}}_0) p_1(\vec{\mathbf{X}}_1) \quad (25)$$

$$= \frac{1}{Z_0} q_0(\vec{\mathbf{X}}_0) \exp(-k\varepsilon(\vec{\mathbf{X}}_0)) \frac{1}{Z_1} q_1(\vec{\mathbf{X}}_1) \exp(-k\varepsilon(\vec{\mathbf{X}}_1)) \quad (26)$$

$$= \frac{1}{Z_0 Z_1} q(\vec{\mathbf{X}}_0, \vec{\mathbf{X}}_1) \exp(-k(\varepsilon(\vec{\mathbf{X}}_0) + \varepsilon(\vec{\mathbf{X}}_1))), \quad (27)$$

where in the first and third equality we use the definition of independent variables, while in the second equality the assumption of Eq. 14 is applied.

Therefore, the marginal density p_t is given by:

$$p_t(\vec{\mathbf{X}}_t) = \iint p_t(\vec{\mathbf{X}}_t | \vec{\mathbf{X}}_0, \vec{\mathbf{X}}_1) p(\vec{\mathbf{X}}_0, \vec{\mathbf{X}}_1) d\vec{\mathbf{X}}_0 d\vec{\mathbf{X}}_1 \quad (28)$$

$$= \iint q_t(\vec{\mathbf{X}}_t | \vec{\mathbf{X}}_0, \vec{\mathbf{X}}_1) q(\vec{\mathbf{X}}_0, \vec{\mathbf{X}}_1) \frac{\exp(-k(\varepsilon(\vec{\mathbf{X}}_0) + \varepsilon(\vec{\mathbf{X}}_1)))}{Z_0 Z_1} d\vec{\mathbf{X}}_0 d\vec{\mathbf{X}}_1 \quad (29)$$

$$= \iint q_t(\vec{\mathbf{X}}_0, \vec{\mathbf{X}}_1 | \vec{\mathbf{X}}_t) q_t(\vec{\mathbf{X}}_t) \frac{\exp(-k(\varepsilon(\vec{\mathbf{X}}_0) + \varepsilon(\vec{\mathbf{X}}_1)))}{Z_0 Z_1} d\vec{\mathbf{X}}_0 d\vec{\mathbf{X}}_1 \quad (30)$$

$$= q_t(\vec{\mathbf{X}}_t) \mathbb{E}_{q_t(\cdot, \cdot | \vec{\mathbf{X}}_t)} \left[\frac{\exp(-k(\varepsilon(\vec{\mathbf{X}}_0) + \varepsilon(\vec{\mathbf{X}}_1)))}{Z_0 Z_1} \right], \quad (31)$$

where in the first equality we use the assumption that probability paths p_t and q_t share the same conditional distribution given $\vec{\mathbf{X}}_0, \vec{\mathbf{X}}_1$. Considering the assumption that p_t admits the Boltzmann-like form as in Eq. 14, it can be easily verified that Eq. 15 holds.

Moreover, take the gradient of Eq. 15 with regard to $\vec{\mathbf{X}}_t$ and the intermediate force field is given by:

$$\nabla \varepsilon_t(\vec{\mathbf{X}}_t) = - \frac{\iint \exp(-k(\varepsilon(\vec{\mathbf{X}}_0) + \varepsilon(\vec{\mathbf{X}}_1))) \nabla q_t(\vec{\mathbf{X}}_0, \vec{\mathbf{X}}_1 | \vec{\mathbf{X}}_t) d\vec{\mathbf{X}}_0 d\vec{\mathbf{X}}_1}{k \mathbb{E}_{q_t(\cdot, \cdot | \vec{\mathbf{X}}_t)} [\exp(-k(\varepsilon(\vec{\mathbf{X}}_0) + \varepsilon(\vec{\mathbf{X}}_1)))]}, \quad (32)$$

where we assume that the integrals and gradients can be commuted as in Eq. 23. The numerator can be further expanded by:

$$\iint \exp(-k(\varepsilon(\vec{\mathbf{X}}_0) + \varepsilon(\vec{\mathbf{X}}_1))) \nabla q_t(\vec{\mathbf{X}}_0, \vec{\mathbf{X}}_1 | \vec{\mathbf{X}}_t) d\vec{\mathbf{X}}_0 d\vec{\mathbf{X}}_1 \quad (33)$$

$$= \iint \exp(-k(\varepsilon(\vec{\mathbf{X}}_0) + \varepsilon(\vec{\mathbf{X}}_1))) q_t(\vec{\mathbf{X}}_0, \vec{\mathbf{X}}_1 | \vec{\mathbf{X}}_t) \nabla \log q_t(\vec{\mathbf{X}}_0, \vec{\mathbf{X}}_1 | \vec{\mathbf{X}}_t) d\vec{\mathbf{X}}_0 d\vec{\mathbf{X}}_1 \quad (34)$$

$$= \iint \exp(-k(\varepsilon(\vec{\mathbf{X}}_0) + \varepsilon(\vec{\mathbf{X}}_1))) q_t(\vec{\mathbf{X}}_0, \vec{\mathbf{X}}_1 | \vec{\mathbf{X}}_t) \nabla \log \frac{q_t(\vec{\mathbf{X}}_t | \vec{\mathbf{X}}_0, \vec{\mathbf{X}}_1) q(\vec{\mathbf{X}}_0, \vec{\mathbf{X}}_1)}{q_t(\vec{\mathbf{X}}_t)} d\vec{\mathbf{X}}_0 d\vec{\mathbf{X}}_1 \quad (35)$$

$$= \mathbb{E}_{q_t(\cdot, \cdot | \vec{\mathbf{X}}_t)} [\exp(-k(\varepsilon(\vec{\mathbf{X}}_0) + \varepsilon(\vec{\mathbf{X}}_1))) (\nabla \log q_t(\vec{\mathbf{X}}_t | \vec{\mathbf{X}}_0, \vec{\mathbf{X}}_1) - \nabla \log q_t(\vec{\mathbf{X}}_t))]. \quad (36)$$

Substitute the numerator back into Eq. 32 and the conclusion holds. \square

Proof of Proposition 4.3. We first check whether the continuity condition holds when $t \rightarrow 0^+$. Note that under this condition, the density $q_t(\vec{\mathbf{X}}_0, \vec{\mathbf{X}}_1 | \vec{\mathbf{X}}_t)$ involves into the Dirac mass $\delta(\vec{\mathbf{X}}_t - \vec{\mathbf{X}}_0)$ at point $\vec{\mathbf{X}}_t$, subsequently we have:

$$\lim_{t \rightarrow 0^+} \nabla \varepsilon_t(\vec{\mathbf{X}}_t) = - \lim_{t \rightarrow 0^+} \frac{\iint \exp(-k(\varepsilon(\vec{\mathbf{X}}_0) + \varepsilon(\vec{\mathbf{X}}_1))) \delta(\vec{\mathbf{X}}_t - \vec{\mathbf{X}}_0) d\vec{\mathbf{X}}_0 d\vec{\mathbf{X}}_1}{k \iint \exp(-k(\varepsilon(\vec{\mathbf{X}}_0) + \varepsilon(\vec{\mathbf{X}}_1))) \delta(\vec{\mathbf{X}}_t - \vec{\mathbf{X}}_0) d\vec{\mathbf{X}}_0 d\vec{\mathbf{X}}_1} \quad (37)$$

$$= - \lim_{t \rightarrow 0^+} \frac{\nabla \iint \exp(-k(\varepsilon(\vec{\mathbf{X}}_0) + \varepsilon(\vec{\mathbf{X}}_1))) \delta(\vec{\mathbf{X}}_t - \vec{\mathbf{X}}_0) d\vec{\mathbf{X}}_0 d\vec{\mathbf{X}}_1}{k \int \exp(-k(\varepsilon(\vec{\mathbf{X}}_t) + \varepsilon(\vec{\mathbf{X}}_1))) d\vec{\mathbf{X}}_1} \quad (38)$$

$$= - \lim_{t \rightarrow 0^+} \frac{\nabla \int \exp(-k(\varepsilon(\vec{\mathbf{X}}_t) + \varepsilon(\vec{\mathbf{X}}_1))) d\vec{\mathbf{X}}_1}{k \int \exp(-k(\varepsilon(\vec{\mathbf{X}}_t) + \varepsilon(\vec{\mathbf{X}}_1))) d\vec{\mathbf{X}}_1} \quad (39)$$

$$= - \lim_{t \rightarrow 0^+} \frac{\nabla \exp(-k\varepsilon(\vec{\mathbf{X}}_t))}{k \exp(-k\varepsilon(\vec{\mathbf{X}}_t))} = \nabla \varepsilon(\vec{\mathbf{X}}_0). \quad (40)$$

The case when t approaches 1 is completely symmetrical and will not be elaborated further. Thus we have proven that the intermediate force field converges to the MD force field when t approaches 0 and 1.

Proof of Proposition 4.4. Given $v'(\vec{\mathbf{X}}_t, t)$ the vector field that generates probability path p_t , according to Eq. 10 we have:

$$v'(\vec{\mathbf{X}}_t, t) = \mathbb{E}_{p_t(\cdot, \cdot | \vec{\mathbf{X}}_t)} \left[\frac{\vec{\mathbf{X}}_1 - \vec{\mathbf{X}}_t}{1 - t} \right]. \quad (41)$$

Similar to Eq. 8, we denote $u'(\vec{\mathbf{X}}_t, t)$ the vector field as the unbiased estimation of the drift term of the reverse-time diffusion process of p_t . Still, we have;

$$u'(\vec{\mathbf{X}}_t, t) = \mathbb{E}_{p_t(\cdot, \cdot | \vec{\mathbf{X}}_t)} \left[\frac{\vec{\mathbf{X}}_t - \vec{\mathbf{X}}_0}{t} \right]. \quad (42)$$

Further, the marginal scores of probability paths q_t, p_t at diffusion time t (termed as s_t^* and s_t' respectively) are connected based on Eq. 14 as follows:

$$s_t'(\vec{\mathbf{X}}_t) = s_t^*(\vec{\mathbf{X}}_t) - k \nabla \varepsilon_t(\vec{\mathbf{X}}_t). \quad (43)$$

Considering the linkage between scores and vector fields in Eq. 7, we obtain:

$$-k \nabla \varepsilon_t(\vec{\mathbf{X}}_t) = \frac{v'(\vec{\mathbf{X}}_t, t) - u'(\vec{\mathbf{X}}_t, t)}{\sigma^2} - \frac{v^*(\vec{\mathbf{X}}_t, t) - u^*(\vec{\mathbf{X}}_t, t)}{\sigma^2} \quad (44)$$

$$= \frac{1}{\sigma^2} [(v'(\vec{\mathbf{X}}_t, t) - v^*(\vec{\mathbf{X}}_t, t)) - (u'(\vec{\mathbf{X}}_t, t) - u^*(\vec{\mathbf{X}}_t, t))]. \quad (45)$$

Now we investigate the intrinsic properties of $v' - v^*$ by expanding the term:

$$v'(\vec{\mathbf{X}}_t, t) - v^*(\vec{\mathbf{X}}_t, t) \quad (46)$$

$$= \frac{1}{1-t} \iint \left(\frac{p_t(\vec{\mathbf{X}}_t | \vec{\mathbf{X}}_0, \vec{\mathbf{X}}_1) p(\vec{\mathbf{X}}_0, \vec{\mathbf{X}}_1)}{p_t(\vec{\mathbf{X}}_t)} - \frac{q_t(\vec{\mathbf{X}}_t | \vec{\mathbf{X}}_0, \vec{\mathbf{X}}_1) q(\vec{\mathbf{X}}_0, \vec{\mathbf{X}}_1)}{q_t(\vec{\mathbf{X}}_t)} \right) \vec{\mathbf{X}}_1 d\vec{\mathbf{X}}_0 d\vec{\mathbf{X}}_1 \quad (47)$$

$$= \frac{1}{(1-t)q_t(\vec{\mathbf{X}}_t)} \iint \vec{\mathbf{X}}_1 q_t(\vec{\mathbf{X}}_t | \vec{\mathbf{X}}_0, \vec{\mathbf{X}}_1) q(\vec{\mathbf{X}}_0, \vec{\mathbf{X}}_1) \left[\frac{Z_t}{Z_0 Z_1} \exp(-k(\varepsilon(\vec{\mathbf{X}}_0) + \varepsilon(\vec{\mathbf{X}}_1) - \varepsilon_t(\vec{\mathbf{X}}_t))) - 1 \right] d\vec{\mathbf{X}}_0 d\vec{\mathbf{X}}_1. \quad (48)$$

Then we define $f(\vec{\mathbf{X}}_0, \vec{\mathbf{X}}_1, \vec{\mathbf{X}}_t, t) = q(\vec{\mathbf{X}}_0, \vec{\mathbf{X}}_1) \left[\frac{Z_t}{Z_0 Z_1} \exp(-k(\varepsilon(\vec{\mathbf{X}}_0) + \varepsilon(\vec{\mathbf{X}}_1) - \varepsilon_t(\vec{\mathbf{X}}_t))) - 1 \right]$, which is symmetric with regard to $\vec{\mathbf{X}}_0, \vec{\mathbf{X}}_1$. Considering the symmetric roles of $\vec{\mathbf{X}}_0$ and $\vec{\mathbf{X}}_1$ in Eq. 15, it is straightforward to conclude that $\varepsilon_t = \varepsilon_{1-t}$ and $Z_t = Z_{1-t}$ for $t \in [0, 1]$. Accordingly, the following equations hold:

$$f(\vec{\mathbf{X}}_0, \vec{\mathbf{X}}_1, \vec{\mathbf{X}}_t, t) = f(\vec{\mathbf{X}}_1, \vec{\mathbf{X}}_0, \vec{\mathbf{X}}_t, t) = f(\vec{\mathbf{X}}_0, \vec{\mathbf{X}}_1, \vec{\mathbf{X}}_t, 1-t). \quad (49)$$

Further, denote $g(\vec{\mathbf{X}}, \vec{\mathbf{X}}_t, t) = \int q_t(\vec{\mathbf{X}}_t | \vec{\mathbf{X}}_0, \vec{\mathbf{X}}) f(\vec{\mathbf{X}}_0, \vec{\mathbf{X}}, \vec{\mathbf{X}}_t, t) d\vec{\mathbf{X}}_0$, Eq. 48 can be rewritten as:

$$v'(\vec{\mathbf{X}}_t, t) - v^*(\vec{\mathbf{X}}_t, t) = \frac{1}{(1-t)q_t(\vec{\mathbf{X}}_t)} \int \vec{\mathbf{X}} g(\vec{\mathbf{X}}, \vec{\mathbf{X}}_t, t) d\vec{\mathbf{X}}. \quad (50)$$

Symmetrically, we can define $h(\vec{\mathbf{X}}, \vec{\mathbf{X}}_t, t) = \int q_t(\vec{\mathbf{X}}_t | \vec{\mathbf{X}}, \vec{\mathbf{X}}_1) f(\vec{\mathbf{X}}, \vec{\mathbf{X}}_1, \vec{\mathbf{X}}_t, t) d\vec{\mathbf{X}}_1$, while $u' - u^*$ admits a similar form of Eq. 50, given by:

$$u'(\vec{\mathbf{X}}_t, t) - u^*(\vec{\mathbf{X}}_t, t) = \frac{-1}{t q_t(\vec{\mathbf{X}}_t)} \int \vec{\mathbf{X}} h(\vec{\mathbf{X}}, \vec{\mathbf{X}}_t, t) d\vec{\mathbf{X}}. \quad (51)$$

Considering the conditional distribution $q_t(\vec{\mathbf{X}}_t | \vec{\mathbf{X}}_0, \vec{\mathbf{X}}_1)$ in the form of Eq. 6 that satisfies $q_t(\vec{\mathbf{X}}_t | \vec{\mathbf{X}}_0, \vec{\mathbf{X}}_1) = q_{1-t}(\vec{\mathbf{X}}_t | \vec{\mathbf{X}}_1, \vec{\mathbf{X}}_0)$, an important observation is:

$$h(\vec{\mathbf{X}}, \vec{\mathbf{X}}_t, t) = g(\vec{\mathbf{X}}, \vec{\mathbf{X}}_t, 1-t). \quad (52)$$

On the other hand, when t approaches 1, the limit of function g is given by:

$$\lim_{t \rightarrow 1^-} g(\vec{\mathbf{X}}, \vec{\mathbf{X}}_t, t) \quad (53)$$

$$= \lim_{t \rightarrow 1^-} \int \delta(\vec{\mathbf{X}}_t - \vec{\mathbf{X}}) q_0(\vec{\mathbf{X}}_0) q_1(\vec{\mathbf{X}}) \left[\frac{Z_t}{Z_0 Z_1} \exp(-k(\varepsilon(\vec{\mathbf{X}}_0) + \varepsilon(\vec{\mathbf{X}}) - \varepsilon_t(\vec{\mathbf{X}}_t))) - 1 \right] d\vec{\mathbf{X}}_0 \quad (54)$$

$$= q_1(\vec{\mathbf{X}}) \int \left[\frac{1}{Z_0} q_0(\vec{\mathbf{X}}_0) \exp(-k\varepsilon(\vec{\mathbf{X}}_0)) - q_0(\vec{\mathbf{X}}_0) \right] d\vec{\mathbf{X}}_0 \quad (55)$$

$$= q_1(\vec{\mathbf{X}}) \int [p_0(\vec{\mathbf{X}}_0) - q_0(\vec{\mathbf{X}}_0)] d\vec{\mathbf{X}}_0 = \mathbf{0}. \quad (56)$$

Suppose the function g is separable with respect to the time variable t . Formally, there exist functions ι and Γ such that the following identity holds:

$$g(\vec{\mathbf{X}}, \vec{\mathbf{X}}_t, t) \equiv \iota(t)\Gamma(\vec{\mathbf{X}}, \vec{\mathbf{X}}_t). \quad (57)$$

Given $\lim_{t \rightarrow 1-} g(\vec{\mathbf{X}}, \vec{\mathbf{X}}_t, t) = \mathbf{0}$, we prescribe $\iota(t) = 1 - t$ for convenience, then we have $h(\vec{\mathbf{X}}, \vec{\mathbf{X}}_t, t) = t\Gamma(\vec{\mathbf{X}}, \vec{\mathbf{X}}_t)$ and subsequently we can derive the closed-form of v' based on Eq. 50 and 51 by:

$$u'(\vec{\mathbf{X}}_t, t) - u^*(\vec{\mathbf{X}}_t, t) = \frac{-1}{tq_t(\vec{\mathbf{X}}_t)} \int \vec{\mathbf{X}} h(\vec{\mathbf{X}}, \vec{\mathbf{X}}_t, t) d\vec{\mathbf{X}} \quad (58)$$

$$= \frac{-1}{q_t(\vec{\mathbf{X}}_t)} \int \vec{\mathbf{X}} \Gamma(\vec{\mathbf{X}}, \vec{\mathbf{X}}_t) d\vec{\mathbf{X}} \quad (59)$$

$$= \frac{-1}{(1-t)q_t(\vec{\mathbf{X}}_t)} \int \vec{\mathbf{X}} (1-t)\Gamma(\vec{\mathbf{X}}, \vec{\mathbf{X}}_t) d\vec{\mathbf{X}} \quad (60)$$

$$= -(v'(\vec{\mathbf{X}}_t, t) - v^*(\vec{\mathbf{X}}_t, t)), \quad (61)$$

such that $v'(\vec{\mathbf{X}}_t, t) = v^*(\vec{\mathbf{X}}_t, t) - \frac{\sigma^2}{2} k \nabla \varepsilon_t(\vec{\mathbf{X}}_t)$ according to Eq. 44. \square

C MODEL ARCHITECTURE

In this work, we leverage the powerful TorchMD-NET (Pelaez et al., 2024) as the backbone model to process molecular graphs, which intrinsically satisfies SO(3)-equivariance with the *equivariant transformer* (Thölke & Fabritiis, 2022) component. To adapt to our task setup, the inputs include not only the Cartesian coordinates $\vec{\mathbf{X}}$ and atom embeddings \mathbf{Z} , but also a one-dimensional continuous diffusion time t . TorchMD-NET will then output SO(3)-equivariant vectors $\vec{\mathbf{V}} \in \mathbb{R}^{N \times 3 \times H}$ and node representations $\mathbf{H} \in \mathbb{R}^{N \times H}$. Formally, we have:

$$\vec{\mathbf{V}}, \mathbf{H} = \text{TorchMD-NET}(\vec{\mathbf{X}}, \mathbf{Z}, t). \quad (62)$$

To streamline the model, we only add lightweight output heads to a single TorchMD-NET module for the baseline model as well as FBM. For the baseline model, we use two separate two-layer Feed-Forward Networks (FFN) with no shared weights to transform the node representations into weights of vectors, which are then multiplied by $\vec{\mathbf{V}}$ to obtain the final representation:

$$v(\vec{\mathbf{X}}, t), u(\vec{\mathbf{X}}, t) := \vec{\mathbf{V}} \times \text{FFN}(\mathbf{H}) \in \mathbb{R}^{N \times 3}, \quad (63)$$

where the dimensions of hidden and output layers of FFN are all H and we use SiLU (Dong et al., 2017) for activation layers. Further, we construct the networks α, β, γ of FBM in the same way, while the only difference is that we add one LayerNorm (Ba et al., 2016) before the FFN layer due to the variance in scale of different targets.

D TRAINING AND INFERENCE DETAILS

In this section, we provide additional details and pseudo codes for training and inference of the baseline bridge matching model FBM-BASE and the force-guided bridge matching model FBM.

D.1 NORMALIZATION OF ENERGIES AND FORCES

In practice, we found that the unnormalized potential function is numerically unstable and its variance is positively correlated with the number of atoms N . To enable stable training, we need to perform special normalization. Specifically, for potential values in kJ/mol, we divide by $3N$ to approximate the standard normal distribution, where N varies with different peptides. For force fields in kJ/mol·nm, due to their relatively stable values across different molecular systems, we simply multiply by the constant 0.002 as the input for training.

D.2 GUIDANCE STRENGTH η

Similar to Wang et al. (2024), we introduce the *guidance strength* η for better approximation of the Boltzmann distribution. Formally, for any positive constant $\eta > 0$, we can define a new probability path based on q_t :

$$p_t(\vec{\mathbf{X}}_t) = \frac{1}{Z_t} q_t(\vec{\mathbf{X}}_t) \exp(-\frac{2\eta}{\sigma^2} k\varepsilon_t(\vec{\mathbf{X}}_t)), \varepsilon_0 = \varepsilon_1 = \varepsilon. \quad (64)$$

The only difference with Eq. 14 is the constant $2\eta/\sigma^2$ in the exponential term, which can be interpreted as how well the probability path p_t is guided by energies and forces. According to Prop. 4.4, it can be easily deduced that the vector field $v'(\vec{\mathbf{X}}_t, t)$ which generates p_t has the following form:

$$v'(\vec{\mathbf{X}}_t, t) = v^*(\vec{\mathbf{X}}_t, t) - \eta \cdot k\varepsilon_t(\vec{\mathbf{X}}_t). \quad (65)$$

Thus practically, we regard η as a hyperparameter during inference and enhance the similarity between p_t and the Boltzmann distribution by selecting the proper guidance strength η .

D.3 REFINEMENT WITH CONSTRAINED ENERGY MINIMIZATION

We utilize the discrete form of the SDE process in Eq. 4 for inference with T SDE steps, and the full conformation ensembles are generated in an autoregressive way, where the output from the previous step serves as the input for the next step. However, in the autoregressive fashion, errors at each inference step will accumulate, leading to out-of-distribution problem. Here we introduce an additional energy minimization procedure using `OpenMM` (Eastman et al., 2017) for refinement, which is performed for each generated conformation before sent to the next inference step. Note that we aim for the refinement to affect only the minor details (e.g., X-H bonds) without altering the overall conformation; therefore, independent harmonic constraints are further applied on all heavy atoms with spring constant of $10 \text{ kcal/mol}\cdot\text{\AA}^2$ and the tolerance of $2.39 \text{ kcal/mol}\cdot\text{\AA}^2$ without maximal step limits (Wang et al., 2024).

D.4 ALGORITHMS FOR TRAINING AND INFERENCE

We provide pseudo codes for training and inference with our models FBM-BASE and FBM in Algorithm 1,2,3 respectively.

Algorithm 1 Training with FBM-BASE

```

1: Input: peptide pairs  $(\mathcal{G}_0, \mathcal{G}_1)$  in a batch  $B$ , vector field networks  $u(\vec{\mathbf{X}}_t, t), v(\vec{\mathbf{X}}_t, t)$ 
2: for training iterations do
3:    $t \sim \text{Uni}(0, 1)$ 
4:    $\vec{\mathbf{X}}_t \sim q_t(\vec{\mathbf{X}}_t | \vec{\mathbf{X}}_0, \vec{\mathbf{X}}_1)$ 
5:    $\hat{\vec{\mathbf{X}}}_0 \leftarrow \vec{\mathbf{X}}_t - tu(\vec{\mathbf{X}}_t, t), \hat{\vec{\mathbf{X}}}_1 \leftarrow \vec{\mathbf{X}}_t + (1-t)v(\vec{\mathbf{X}}_t, t)$ 
6:    $(D_0, D_1, \hat{D}_0, \hat{D}_1) \leftarrow$  pairwise interatomic distances of  $(\vec{\mathbf{X}}_0, \vec{\mathbf{X}}_1, \hat{\vec{\mathbf{X}}}_0, \hat{\vec{\mathbf{X}}}_1)$ 
7:    $\mathcal{L}_{\text{fwd}} \leftarrow \frac{1}{B} \sum_{\mathcal{G}_0, \mathcal{G}_1} \|(\vec{\mathbf{X}}_1 - \vec{\mathbf{X}}_t)/(1-t) - v(\vec{\mathbf{X}}_t, t)\|^2$ 
8:    $\mathcal{L}_{\text{rev}} \leftarrow \frac{1}{B} \sum_{\mathcal{G}_0, \mathcal{G}_1} \|(\vec{\mathbf{X}}_t - \vec{\mathbf{X}}_0)/t - u(\vec{\mathbf{X}}_t, t)\|^2$ 
9:    $\mathcal{L}_{\text{aux}} \leftarrow \frac{1}{B} \sum_{\mathcal{G}_0, \mathcal{G}_1} (1-t) \cdot \frac{\|\mathbf{1}_{D_0 < 6\text{\AA}}(D_0 - \hat{D}_0)\|^2}{\sum \mathbf{1}_{D_0 < 6\text{\AA}} - N} + t \cdot \frac{\|\mathbf{1}_{D_1 < 6\text{\AA}}(D_1 - \hat{D}_1)\|^2}{\sum \mathbf{1}_{D_1 < 6\text{\AA}} - N}$ 
10:   $\mathcal{L}_{\text{base}} \leftarrow \mathcal{L}_{\text{fwd}} + \mathcal{L}_{\text{rev}} + 0.25 \cdot \mathcal{L}_{\text{aux}}$ 
11:   $\min \mathcal{L}_{\text{base}}$ 
12: end for
```

D.5 HYPERPARAMETERS

The hyperparameters we choose are listed in Table 3.

Algorithm 2 Training with FBM

```

1: Input: peptide pairs  $(\mathcal{G}_0, \mathcal{G}_1)$  of one molecular system in a batch  $B$ , baseline model
    $v^*(\vec{\mathbf{X}}_t, t), u^*(\vec{\mathbf{X}}_t, t)$  in § 4.2 with frozen parameters, MD potentials  $\varepsilon(\vec{\mathbf{X}}_0), \varepsilon(\vec{\mathbf{X}}_1)$ , MD force
   fields  $\nabla\varepsilon(\vec{\mathbf{X}}_0), \nabla\varepsilon(\vec{\mathbf{X}}_1)$ , force field networks  $\alpha(\vec{\mathbf{X}}_t, t), \beta(\vec{\mathbf{X}}_t, t), \gamma(\vec{\mathbf{X}}_t, t)$ 
2: for training iterations do
3:    $t \sim \text{Uni}(0, 1)$ 
4:    $\vec{\mathbf{X}}_t \sim q_t(\vec{\mathbf{X}}_t | \vec{\mathbf{X}}_0, \vec{\mathbf{X}}_1)$ 
5:    $s_t^*(\vec{\mathbf{X}}_t) \leftarrow (v^*(\vec{\mathbf{X}}_t, t) - u^*(\vec{\mathbf{X}}_t, t)) / \sigma^2$ 
6:    $\zeta(\vec{\mathbf{X}}_0, \vec{\mathbf{X}}_1, \vec{\mathbf{X}}_t) \leftarrow s_t^*(\vec{\mathbf{X}}_t) - \nabla \log q_t(\vec{\mathbf{X}}_t | \vec{\mathbf{X}}_0, \vec{\mathbf{X}}_1)$ 
7:    $M \leftarrow \frac{1}{B} \sum_{\mathcal{G}_0, \mathcal{G}_1} q_t(\vec{\mathbf{X}}_t | \vec{\mathbf{X}}_0, \vec{\mathbf{X}}_1) \exp(-k(\varepsilon(\vec{\mathbf{X}}_0) + \varepsilon(\vec{\mathbf{X}}_1)))$ 
8:    $w(\vec{\mathbf{X}}_t, t) \leftarrow (1 - t) \cdot \text{detach}(\alpha(\vec{\mathbf{X}}_t, t)) + t \cdot \text{detach}(\beta(\vec{\mathbf{X}}_t, t)) + t(1 - t) \cdot \gamma(\vec{\mathbf{X}}_t, t)$ 
9:    $\mathcal{L}_{\text{diff}} \leftarrow \frac{1}{B} \sum_{\mathcal{G}_0, \mathcal{G}_1} \|\exp(-k(\varepsilon(\vec{\mathbf{X}}_0) + \varepsilon(\vec{\mathbf{X}}_1))) \zeta(\vec{\mathbf{X}}_0, \vec{\mathbf{X}}_1, \vec{\mathbf{X}}_t) / kM - w(\vec{\mathbf{X}}_t, t)\|^2$ 
10:   $\mathcal{L}_{\text{bnd}} \leftarrow \frac{1}{B} \sum_{\mathcal{G}_0, \mathcal{G}_1} \|\nabla\varepsilon(\vec{\mathbf{X}}_0) - \alpha(\vec{\mathbf{X}}_t, t)\|^2 + \|\nabla\varepsilon(\vec{\mathbf{X}}_1) - \beta(\vec{\mathbf{X}}_t, t)\|^2$ 
11:   $\mathcal{L}_{\text{FBM}} \leftarrow \mathcal{L}_{\text{diff}} + \mathcal{L}_{\text{bnd}}$ 
12:   $\min \mathcal{L}_{\text{FBM}}$ 
13: end for

```

Algorithm 3 Autoregressive inference with FBM/FBM-BASE

```

1: Input: Initial state  $\mathcal{G}_0$ , chain length  $L$ , discrete SDE step  $T$ , guidance strength  $\eta$ , baseline model
    $v(\vec{\mathbf{X}}_t, t)$  in § 4.2, FBM model  $w(\vec{\mathbf{X}}_t, t)$  in § 4.3, model type  $c \in \{\text{FBM-BASE}, \text{FBM}\}$ 
2:  $C \leftarrow []$ 
3:  $\Delta \leftarrow 1/T$ 
4: for  $l \leftarrow 1$  to  $L$  do
5:   for  $t$  in  $\text{linspace}(0, 1 - \Delta, T)$  do
6:      $\epsilon \sim \mathcal{N}(\mathbf{0}, I)$ 
7:     if  $c = \text{FBM}$  then
8:        $v'(\vec{\mathbf{X}}_t, t) \leftarrow v(\vec{\mathbf{X}}_t, t) - \eta \cdot kw(\vec{\mathbf{X}}_t, t)$ 
9:     else
10:       $v'(\vec{\mathbf{X}}_t, t) \leftarrow v(\vec{\mathbf{X}}_t, t)$ 
11:    end if
12:     $\vec{\mathbf{X}}_{t+\Delta} \leftarrow \vec{\mathbf{X}}_t + v'(\vec{\mathbf{X}}_t, t)\Delta + \sqrt{t}\sigma\epsilon$ 
13:  end for
14:   $\vec{\mathbf{X}}'_1 \leftarrow \text{energy\_minim}(\vec{\mathbf{X}}_1)$ 
15:   $\vec{\mathbf{X}}_0 \leftarrow \vec{\mathbf{X}}'_1$ 
16:   $C \leftarrow C \cup \vec{\mathbf{X}}_1$ 
17: end for
18: Output  $C$ 

```

E EXPERIMENTAL DETAILS**E.1 DATASET DETAILS**

As mentioned in § 5.1, all peptides of PepMD are simulated in explicit solvent model TIP3PFB using OpenMM (Eastman et al., 2017). The parameters we used for MD simulation are listed in Table 4 and the statistical information of PepMD is shown in Table 5.

Additionally, all 14 peptides of our test set are listed below with the format {pdb-id}:{chain-id}:
 1hhg:C, 1k8d:P, 1k83:M, 1bz9:C, 1i7u:C, 1gxc:B, 1ar8:O, 2xa7:P, 1e28:C, 1gy3:F, 1n73:I, 1fpr:B,
 1aze:B, 1qj6:I.

E.2 DETAILS ON EVALUATION METRICS

In this part, we provide details for computing the evaluation metrics in § 5.1.

Table 3: Hyperparameter choice of FBM-BASE and FBM.

Hyperparameters	Values
Network	
Hidden dimension H of FBM-BASE	128
Hidden dimension H of FBM	176
RBF dimension	32
Number of attention heads	8
Number of layers	6
Cutoff threshold r_{cut}	5.0 Å
Training	
Learning rate	5e-4
Optimizer	Adam
Warm up steps	1,000
Warm up scheduler	LamdaLR
Training scheduler	ReduceLROnPlateau(factor=0.8, patience=5, min.lr=1e-7)
Batch size of FBM-BASE	16
Batch size of FBM	10
SDE noise scale σ	0.2
Inference	
SDE steps T	[25,30]
Guidance strength η of FBM	[0.04,0.05,0.06,0.07,0.08]

Table 4: MD simulation setups using OpenMM.

Property	Value
Forcefield	AMBER-14
Integrator	LangevinMiddleIntegrator
Integration time step	1fs
Frame spacing	1ps
Friction coefficient	1.0ps ⁻¹
Temperature	300K
Solvation	TIP3PFB
Electrostatics	NoCutoff
Constraints	all bonds between hydrogens

Flexibility Following Janson et al. (2023), we compute the contact rates between residues as a measure of structural flexibility. For each residue pair i, j ($1 \leq i < j \leq R$) of a peptide with R residues, the contact rate $r(i, j)$ of residue i, j is defined as follows:

$$r(i, j) = \frac{1}{L} \sum_{l=1}^L \mathbf{1}_{d_l(i, j) < 10 \text{ Å}}, \quad (66)$$

where $d_l(i, j)$ denotes the Euclidean distance between α -carbons of residue i, j of conformation l . Now we compute the root mean square error of contact maps between generated ensembles and reference MD trajectories:

$$\text{CONTACT} = \sqrt{\frac{2}{R(R-1)} \sum_{1 \leq i < j \leq R} (r(i, j) - r_{\text{ref}}(i, j))^2}. \quad (67)$$

Table 5: Dataset statistics.

Dataset name	PepMD
Training set simulation time	100ns
Test set simulation time	100ns
MD integration time step Δt	1fs
coarsened prediction time τ	0.5×10^6 fs
# Clusters	2480
# Training peptides	136
# Training pairs per peptide	2×10^3
# Validation pairs per peptide	4×10^2
# Test peptides	14

Validity We assess the structural validity by checking for bond breaks between adjacent residues and bond clashes between any residue pairs. The same as in Wang et al. (2024), *bond clash* occurs when the distance between α -carbons of any residue pair is less than the threshold $\delta_{\text{clash}} = 3.0\text{\AA}$, and *bond break* occurs when the distance between adjacent α -carbons is greater than the threshold $\delta_{\text{break}} = 4.19\text{\AA}$. Then the metric VAL-CA is assessed by the fraction of conformations without bond break and bond clash.

Distributional Similarity Similar to Lu et al. (2023b), we project peptide conformations onto the following three low-dimensional feature space: (i) Pairwise Distance (PWD) between α -carbons excluding residue pairs within an offset of 3. (ii) Radius of gyration (RG) which computes the geometric mean of the distances from α -carbons to the center-of-mass. (iii) Time-lagged Independent Components (TIC), where we featurize structures using backbone dihedrals ψ, ϕ, ω and pairwise distances between α -carbons (Klein et al., 2024), then TIC analysis is performed using Deeptime (Hoffmann et al., 2021). Only the slowest components, TIC 0 and TIC 1, are taken for further evaluation (Pérez-Hernández et al., 2013). (iv) the joint distribution of TIC 0 and TIC 1, termed as TIC-2D. (v) Specifically for the evaluation on AD, the joint distribution of backbone dihedrals ψ and ϕ , namely the *Ramachandran plot* (Ramachandran et al., 1963), is taken into consideration (RAM).

Afterwards we compute the Jensen-Shannon (JS) distance between generated samples and reference MD trajectories on the projection space. Features are discretized with 50 bins based on the reference ensembles, and a pseudo count $1e-6$ is added for numerical stability. For each feature space, we report the mean distance along all dimensions.

F ADDITIONAL EXPERIMENTAL RESULTS

F.1 ABLATION STUDY

In Table 6 we provide ablation results of SDE steps T and the guidance strength η on test peptides of PepMD.

G COMPUTING INFRASTRUCTURE

Our models, FBM-BASE and FBM, were trained on 4 NVIDIA GeForce RTX 3090 GPUs within a week. The inference procedure with baselines and our model were all performed on one single NVIDIA GeForce RTX 3090 GPU.

Table 6: Ablation results of SDE steps T and the guidance strength η on the test set of PepMD. Values are shown in median/std of all 14 test peptides in a single run.

Hyperparameters	JS DISTANCE (\downarrow)				VAL-CA (\uparrow)	CONTACT (\downarrow)
	PWD	RG	TIC	TIC-2D		
$T = 25, \eta = 0.04$	0.567/0.074	0.529/0.122	0.641/0.080	0.805/0.035	0.789/0.136	0.198/0.132
$T = 25, \eta = 0.05$	0.577/0.072	0.572/0.122	0.643/0.084	0.805/0.033	0.780/0.139	0.199/0.120
$T = 25, \eta = 0.06$	0.573/0.067	0.533/0.156	0.635/0.072	0.798/0.034	0.798/0.135	0.192/0.137
$T = 25, \eta = 0.07$	0.567/0.068	0.546/0.121	0.645/0.077	0.807/0.027	0.814/0.104	0.191/0.107
$T = 25, \eta = 0.08$	0.573/0.064	0.568/0.126	0.641/0.072	0.809/0.025	0.781/0.135	0.200/0.118
$T = 30, \eta = 0.04$	0.595/0.081	0.606/0.131	0.640/0.082	0.807/0.027	0.843/0.123	0.204/0.127
$T = 30, \eta = 0.05$	0.588/0.081	0.558/0.145	0.648/0.069	0.812/0.024	0.806/0.136	0.206/0.120
$T = 30, \eta = 0.06$	0.590/0.065	0.592/0.161	0.655/0.079	0.808/0.026	0.817/0.231	0.208/0.153
$T = 30, \eta = 0.07$	0.592/0.062	0.593/0.147	0.643/0.085	0.810/0.026	0.874/0.081	0.192/0.113
$T = 30, \eta = 0.08$	0.590/0.077	0.595/0.146	0.651/0.073	0.807/0.022	0.851/0.180	0.217/0.134